Neurocomputing 267 (2017) 95–106

Contents lists available at ScienceDirect

Neurocomputing

journal homepage: www.elsevier.com/locate/neucom

Group sparsity based regularization model for remote sensing image stripe noise removal

Yong Chen*, Ting-Zhu Huang*, Liang-Jian Deng, Xi-Le Zhao, Min Wang

School of Mathematical Sciences/Research Center for Image and Vision Computing, University of Electronic Science and Technology of China, Chengdu, Sichuan 611731, China

ARTICLE INFO

Article history:
Received 23 December 2016
Revised 18 March 2017
Accepted 1 May 2017
Available online 15 May 2017

Communicated by Dr. Y Gu

Keywords:
Convex optimization
Group sparsity
Alternating direction method of multipliers
Remote sensing image
Image destriping

ABSTRACT

Stripe noise degradation is a common phenomenon in remote sensing image, which largely affects the visual quality and brings great difficulty for subsequent processing. In contrast to existing stripe noise removal (destriping) models in which the reconstruction is performed to directly estimate the clean image from the striped one, the proposed model achieves the destriping by estimating the stripe component firstly. Since the stripe component possesses column sparse structure, the group sparsity is employed in this study. In addition, difference-based constraints are used to describe the direction information of the stripes. Then, we build a novel convex optimization model which consists of a unidirectional total variation term, a group sparsity term and a gradient domain fidelity term solved by an efficient alternating direction method of multiplier. Compared with the state-of-the-art methods, experiment results on simulated and real data are reported to demonstrate the effectiveness of the proposed method.

1. Introduction

Remote sensing image plays an important role in many fields, such as urban planning, military, and environment monitoring. However, different sensors produce inconsistent responses in the imaging process, which leads to the images degraded by stripe noise. The stripe noise existing in remote sensing image badly degrades the visual quality and restricts the precision in data analysis, such as unmixing [1], classification [2], and target detection [3]. To reduce the unfavorable effects caused by stripe noise, it is critical to develop efficient methods to remove the stripes before subsequent applications. The goal of this work is to separate the stripe component and preserve the stripe-free information.

In recent decades, a lot of destriping methods have been proposed. Extensively existing destriping methods can be roughly divided into three categories: digit filtering-based methods, statistics-based methods, and optimization-based methods. It is worth mentioning that these methods sometimes have overlap among this categories. For instance, some optimization-based methods may involve statistics-based methodological ideas.

One straightforward idea for image destriping is filtering. These filtering-based methods remove stripes by constructing a filter on a transformed domain, e.g., Fourier domain filter [4–6], wavelet analysis [7,8] and the Fourier-wavelet combined domain filter [9,10]. These methods suppose that the stripes are periodic and can be clearly discovered from the power spectrum. However, some evident details with the similar features to the stripes also exist in the stripe-free regions, these details would be excessively filtered out, which results in blurring or artifacts of the output image. In [9], the authors proposed Fourier-wavelet combined domain filter method to remedy this shortage, which better preserves the original image information in the stripe-free locations.

Statistics-based methods are also commonly used for image destriping [11–16]. These methodological ideas assume that the distribution of the digital number for each detector approaches is the same, e.g., moment matching [11,14] and histogram matching [15]. The moment matching considers that the changes of the mean and standard deviation of each sensor are small, if this assumption holds, then these methods can remove stripe noise efficiently. The histogram matching is based on the assumption that the probability distribution of scene radiances seen by each sensor is the same. In general, statistics-based methods are easy to perform, and the computational process is fast, but these methods are greatly determined by the preestablish reference moment or histogram.

At present, optimization-based models have attracted many attentions and are widely applied to image destriping. Regarding the destriping problem as a conventional ill-posed inverse problem [17–21], existing regularization methods are employed to solve the destriping problem by introducing prior information. These methods compute the desired image by minimizing an energy function

* Corresponding authors.
E-mail addresses: chenyong1872008@163.com (Y. Chen), tingzhuhuang@126.com (T.-Z. Huang).

http://dx.doi.org/10.1016/j.neucom.2017.05.018
0925-2312/

under some regularization terms. Shen and Zhang [17] established maximum a posteriori (MAP) framework and added Huber–Markov prior information for destriping and inpainting. In [18], the authors made the advantages of direction information of the stripes and proposed an unidirectional total variation (UTV) model to remove stripe noise. However, the method in [18] recognized the stripe regions and stripe-free regions inaccurately and produced a poor performance on heavy stripe noise. To overcome these weaknesses of UTV model, many researchers have proposed some modified UTV models [19,20,22,23]. In [20], the authors proposed a UTV-Stokes model, which avoids excessive over-smoothing by distinguishing stripe regions and stripe-free regions. In hyperspectral image destriping field, some researchers also considered the low-rank matrix recovery by exploiting the high spectral correlation between the latent image in different bands [24–26]. In [25], the authors proposed the graph regularizer low-rank representation (LRR) destriping method by incorporating the LRR technique, which is the first work to use LRR technique for destriping.

However, most of existing methods focus on directly estimating the clean image from observed one, paying much attention to the image itself, while without considering the directional and structural properties for the stripes, which would result in many image details may be removed along with stripes and residual stripes existing in the latent image. Recently, Liu et al. [27] obtains the destriping image from a novel perspective, which is first to estimate the stripe component and then utilizes the difference between observed image and stripe component to obtain the final destriping image. The global sparsity and local variational properties of the stripe component are considered in [27] to estimate the stripe component. The authors used ℓ_0-norm-based regularization to describe global sparse distribution of the stripes. But the ℓ_0-norm is non-convex, and global sparsity fails to reflect the inner structure of stripe component. Moreover, the sparsity property of stripes has disappeared when the stripes are too dense. To remedy this deficiency, the goal of this work is to focus on exploring stripes prior and achieving better stripe noise removal results.

In this paper, we introduce the group sparsity that is depicted by $\ell_{2,1}$-norm to describe the inner structure of stripe component and generate better results than recent state-of-the-art methods. Actually, the stripe image can be viewed as consisting of clean image and stripe component, and these two components can be regarded as equally. To obtain the clean image, which is equivalent to the problem of estimating the stripe component. Since the stripe component possesses line-by-line structures, we employ $\ell_{2,1}$-norm regularization to preserve the structure. Moreover, as the stripe noise has a clear directional feature, we also consider the differential properties of the along-stripe direction and across-stripe direction. Finally, we propose a novel optimization-based model for remote sensing image destriping problem. To solve the proposed convex model efficiently, an alternating direction method of multipliers (ADMM) based algorithm is developed to solve it. The main ideas and contributions of the proposed method are summarized as follows:

- As the stripe noise has obvious directional and structural properties, we employ these properties to construct a convex sparse optimization model that is solved by ADMM method. In particular, the convergence of the proposed method is guaranteed.
- We explore the group sparsity property of stripe noise in remote sensing image via implementing statistical analysis, and utilize $\ell_{2,1}$-norm regularization to depict the group sparsity property.
- Numerical experimental results, including simulated and real experiments, demonstrate that the proposed method outperforms the state-of-the-art results.

The rest of this paper is organized as follows. In the next section, we present the stripe component properties in details. In Section 3, the proposed model and optimization method are described. Section 4 presents some numerical experiments to demonstrate the effectiveness and satisfactory performance of the proposed method. Finally, we conclude paper in Section 5.

2. Stripe component properties analysis

Unlike other types of noises, the stripe noise has obviously directional and structural properties. How to design an appropriate regularization terms to describe these properties is the key issue in the stripe noise remove problem.

2.1. Problem formulation

The striping effects in remote sensing images are modeled as an additive noise [17,18], and thus the stripes degradation process can be formulated as

$$f(x,y) = u(x,y) + s(x,y), \tag{1}$$

where $f(x, y)$, $u(x, y)$, and $s(x, y)$ represent the degraded image from the detectors, the potential stripe-free image, and the stripe component at the location of (x, y), respectively. For the purpose of discussing numerical algorithm, a matrix-vector form of (1) can be rewritten as follows

$$\mathbf{f} = \mathbf{u} + \mathbf{s}, \tag{2}$$

where $\mathbf{f}$, $\mathbf{u}$, and $\mathbf{s}$ stand for the vectorized discrete version of $f(x, y)$, $u(x, y)$, and $s(x, y)$, respectively. In previous works, most of destriping methods aim to directly compute stripe-free image $\mathbf{u}$ from the degraded image $\mathbf{f}$. However, here we change our perspective to explore the further properties of stripe noise and propose a more efficient method to remove stripe noise and retain pixel values of stripe-free regions. This paper concentrate on extracting the stripe component $\mathbf{s}$ from degraded image $\mathbf{f}$. The framework of the proposed method is illustrated in Fig. 1.

2.2. Directional and structural properties of stripe component

To precisely estimate the stripe component, the key issue now is to excavate the properties of stripe component, and to depict them in appropriate regularization terms. Firstly, we use statistics-based method [16] (SLD) which achieves destriping by estimating the stripe component to remove stripe noise in MODIS image. In the meanwhile, we show the gradients of the stripe image at two directions: horizontal and vertical direction, and the results as shown in Fig. 2. From the results, we can find that the stripe component possesses directional property and structural property.

(1) *Directional property*: Figs. 2(d)–(e) show the gradients of stripe component in horizontal and vertical direction. From which, we can observe that the vertical gradient is quite sparse that indicates the stripe component has good smoothness in vertical direction. To preserve the stripe gradient well in vertical direction, we employ the sparse regularization on gradient domain to constrain it. The best choice is to employ ℓ_0-norm [27] that counts nonzero-element-number or hyper-Laplacian prior distribution that is depicted by ℓ_p-norm $(0 < p < 1)$ [28]. However, these are non-convex problems, and the globally optimal solution is hard to find. In addition, the results of ℓ_0 norm and ℓ_p norm are sensitive to the initial point, and the convergence of algorithm fail to guarantee. Here, we use ℓ_1-norm which is a convex function as the sparse regularization that is given as

$$R_1(\mathbf{s}) = \|\nabla_y \mathbf{s}\|_1, \tag{3}$$

where ∇_y denotes the linear first-order difference operators in vertical direction.

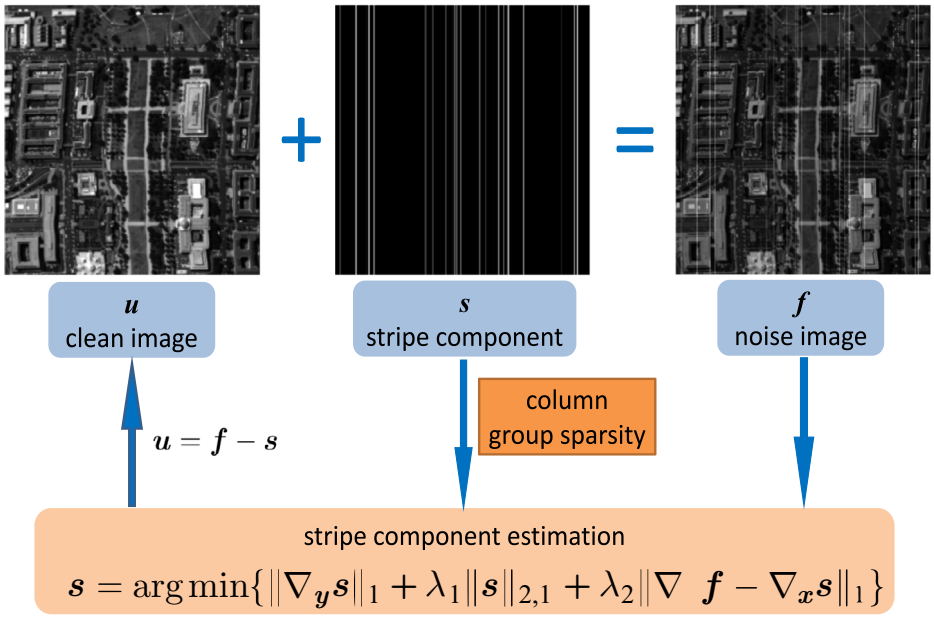

Fig. 1. The framework of the proposed model.

Moreover, Figs. 2(f)–(g) show the gradients of the degraded image at two directions. Due to the existing stripe noise, it may affect the horizontal gradient, while the vertical gradient is not affected seriously. To remove the stripe noise, it requires the horizontal gradient of the desired image **u** smooth. Thus, the unidirectional total variation [18] of the desired image is considered as

$$R_2(\mathbf{s}) = \|\nabla_x \mathbf{u}\|_1 = \|\nabla_x \mathbf{f} - \nabla_x \mathbf{s}\|_1, \tag{4}$$

where ∇_x denotes the linear first-order difference operators in the horizontal direction.

(2) *Structural property*: Furthermore, the stripe component is different with random noise, and it presents special column structure as shown in Fig. 2(c). In [27], the authors considered that the stripe component can be regarded as a sparse matrix with a plenty of zero elements in the stripe-free regions and applied ℓ_0-norm regularizer to the stripe matrix as

$$R(\mathbf{s}) = \|\mathbf{s}\|_0. \tag{5}$$

The sparsity in (5) assumes that sparse elements are distributed randomly, but it fails to consider the inner structure among these elements. Actually, the stripe matrix can be viewed as consisting of column vectors, and each column is regarded as a group. Interestingly, the stripe-free column elements tend to be all zeros, and the stripe columns are all non-zeros. It motivates us to employ group sparsity regularization which depicted by $\ell_{2,1}$-norm [29] to constrain the stripe component, and it is more reasonable than sparsity regularization to preserve the structure of stripe component.

In Fig. 2(h), the horizontal axis denotes the column number, and the vertical axis stands for the 2-norm value of each column. It is obvious that there are few clear impulse which values are greater than the adjacent ones, and the values of most vertical bars are close to zero. In fact, the pixel values are all zeros in stripe-free columns, thus the small values can be regarded as the calculation errors of the model. Therefore, from Fig. 2(g), it demonstrates again that the group sparsity regularization can be better to describe the structural property of stripe component than sparsity regularization. Thus, we have designed the regularization term as

$$R_3(\mathbf{s}) = \|\mathbf{s}\|_{2,1}. \tag{6}$$

3. The proposed method

Here, we will give the proposed model and its optimization procedure. Although there are some similar destriping works [18,27], they fail to take the structural property of stripe component into consideration. However, the stripe component has a significantly column structural property, which is worth considering to separate the stripe component and preserve the stripe-free information in the destriping process.

3.1. The proposed model

Based on the above analysis, the stripe component has significantly directional property and structural property. By combining R_1, R_2 and R_3, we propose the stripe noise removal model as follows

$$\mathbf{s} = \arg\min_{\mathbf{s}} \{\|\nabla_y \mathbf{s}\|_1 + \lambda_1 \|\mathbf{s}\|_{2,1} + \lambda_2 \|\nabla_x \mathbf{f} - \nabla_x \mathbf{s}\|_1\}, \tag{7}$$

where λ_1 and λ_2 are two positive regularization parameters to balance the three terms. For the convenience of discussion, we consider each stripe line as a column. If the stripes are horizontal, we rotate them to make the stripe lines vertically. When stripe component **s** is extracted from the stripe image **f**, the final destriping image can be estimated by the following formula

$$\mathbf{u} = \mathbf{f} - \mathbf{s}. \tag{8}$$

3.2. ADMM optimization

It is difficult to directly solve **s** from (7) since the ℓ_1-norm terms are nondifferentiable and inseparable. To overcome this difficulty, we utilize an efficient algorithm to deal with this nonsmooth and convex optimization model. In previous works, the ADMM algorithm [30–32] is a popular and efficient optimization method to solve convex model, such as ℓ_1-norm-based minimization [33,34] and total variation (TV) model [35–37] in image processing. Therefore, we employ it to optimize the proposed convex destriping model (7).

The basic idea is to convert the unconstrained minimization problem on **s** in (7) into a constrained optimization model. By introducing three auxiliary variables $\mathbf{z} = \nabla_y \mathbf{s}$, $\mathbf{v} = \mathbf{s}$, and $\mathbf{w} = \nabla_x \mathbf{f} -$

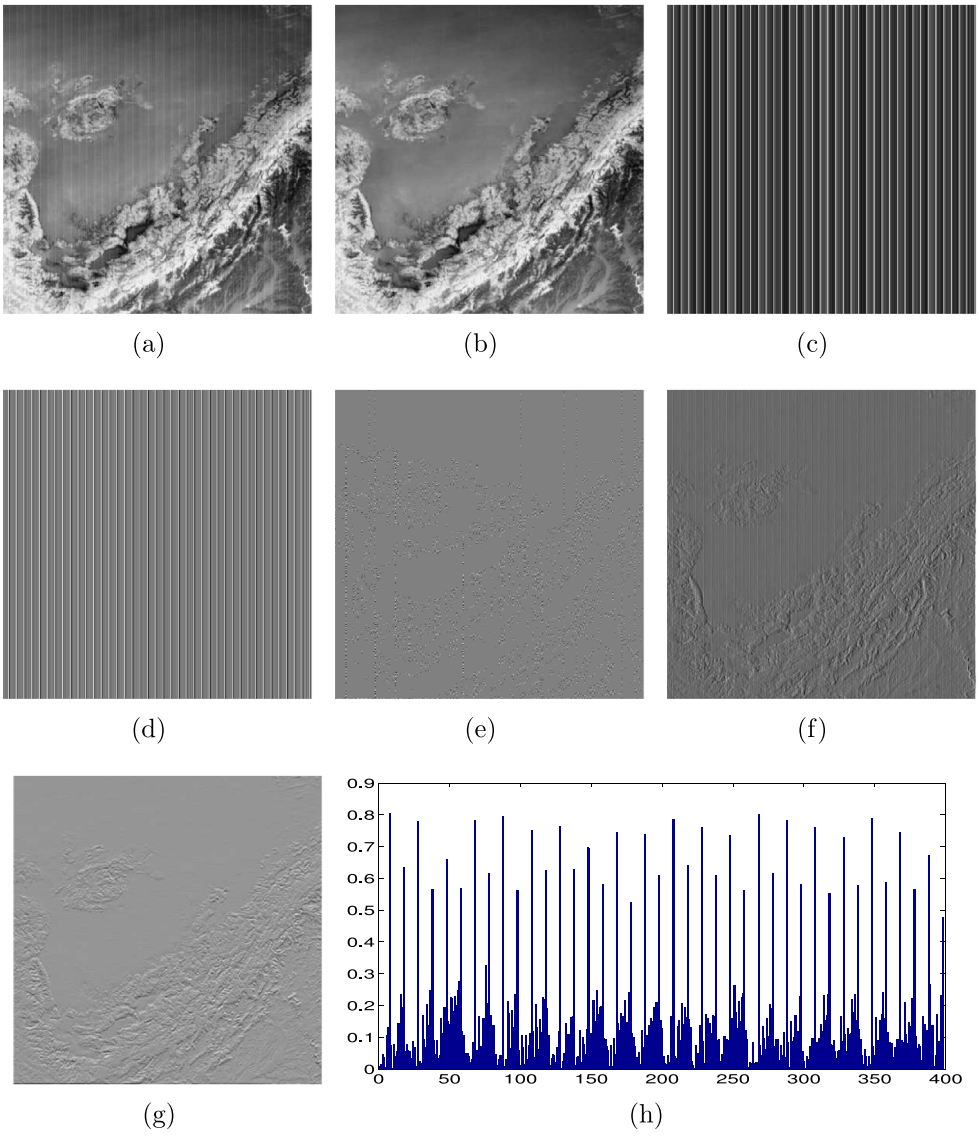

Fig. 2. Destriping results in Terra MODIS band 33 by SLD. (a) Original image; (b) image component; (c) stripe component; (d) horizontal gradient of (c); (e) vertical gradient of (c); (f) horizontal gradient of (a); (g) vertical gradient of (a); (h) the 2-norm each column of (c).

$\nabla_x \mathbf{s}$. The minimization of (7) is equivalent to the constrained problem

$$\begin{aligned} &\arg\min_{\mathbf{s},\mathbf{z},\mathbf{v},\mathbf{w}} \{\|\mathbf{z}\|_1 + \lambda_1\|\mathbf{v}\|_{2,1} + \lambda_2\|\mathbf{w}\|_1\} \\ &s.t.\ \mathbf{z} = \nabla_y \mathbf{s},\ \ \mathbf{v} = \mathbf{s},\ \ \mathbf{w} = \nabla_x \mathbf{f} - \nabla_x \mathbf{s}. \end{aligned} \tag{9}$$

Subsequently, by strictly applying the ADMM algorithm, the (9) can further be converted into the following minimization problem of augmented Lagrange function

$$\begin{aligned} &\arg\min_{\mathbf{s},\mathbf{z},\mathbf{v},\mathbf{w}} \|\mathbf{z}\|_1 + \lambda_1\|\mathbf{v}\|_{2,1} + \lambda_2\|\mathbf{w}\|_1 + p_1^T(\nabla_y \mathbf{s} - \mathbf{z}) \\ &+ p_2^T(\mathbf{s} - \mathbf{v}) + p_3^T(\nabla_x \mathbf{f} \\ &- \nabla_x \mathbf{s} - \mathbf{w}) + \frac{\beta_1}{2}\|\nabla_y \mathbf{s} - \mathbf{z}\|_2^2 + \frac{\beta_2}{2}\|\mathbf{s} - \mathbf{v}\|_2^2 + \frac{\beta_3}{2} \\ &\|\nabla_x \mathbf{f} - \nabla_x \mathbf{s} - \mathbf{w}\|_2^2, \end{aligned} \tag{10}$$

where p_1, p_2, and p_3 denote the Lagrange multipliers; β_1, β_2, and β_3 are three positive penalty parameters. In final, the problem (10) can be solved iteratively and alternatively by solving the following four simpler subproblems.

(1) The $\mathbf{z}$ subproblem is followed by

$$\begin{aligned} \mathbf{z} &= \arg\min_{\mathbf{z}} \left\{\|\mathbf{z}\|_1 + p_1^T(\nabla_y \mathbf{s} - \mathbf{z}) + \frac{\beta_1}{2}\|\nabla_y \mathbf{s} - \mathbf{z}\|_2^2\right\} \\ &= \arg\min_{\mathbf{z}} \left\{\|\mathbf{z}\|_1 + \frac{\beta_1}{2}\|\nabla_y \mathbf{s} - \mathbf{z} + \frac{p_1}{\beta_1}\|_2^2\right\}, \end{aligned} \tag{11}$$

which can be efficiently solved by the following soft-threshold shrinkage operator [38]

$$\mathbf{z}^{k+1} = \mathbf{shrink}\left(\nabla_y \mathbf{s}^k + \frac{p_1^k}{\beta_1}, \frac{1}{\beta_1}\right), \tag{12}$$

where

$$\mathbf{shrink}(r, \theta) = \frac{r}{|r|} * \max(|r| - \theta, 0). \tag{13}$$

(2) Similarly to $\mathbf{z}$ subproblem, the $\mathbf{w}$ subproblem can be easily solved by

$$\begin{aligned} \mathbf{w} &= \arg\min_{\mathbf{w}} \{\lambda_2\|\mathbf{w}\|_1 + p_3^T(\nabla_x \mathbf{f} - \nabla_x \mathbf{s} - \mathbf{w}) + \frac{\beta_3}{2} \\ &\quad \|\nabla_x \mathbf{f} - \nabla_x \mathbf{s} - \mathbf{w}\|_2^2\} \\ &= \arg\min_{\mathbf{w}} \left\{\lambda_2\|\mathbf{w}\|_1 + \frac{\beta_3}{2}\|\nabla_x \mathbf{f} - \nabla_x \mathbf{s} - \mathbf{w} + \frac{p_3}{\beta_3}\|_2^2\right\}, \end{aligned} \tag{14}$$

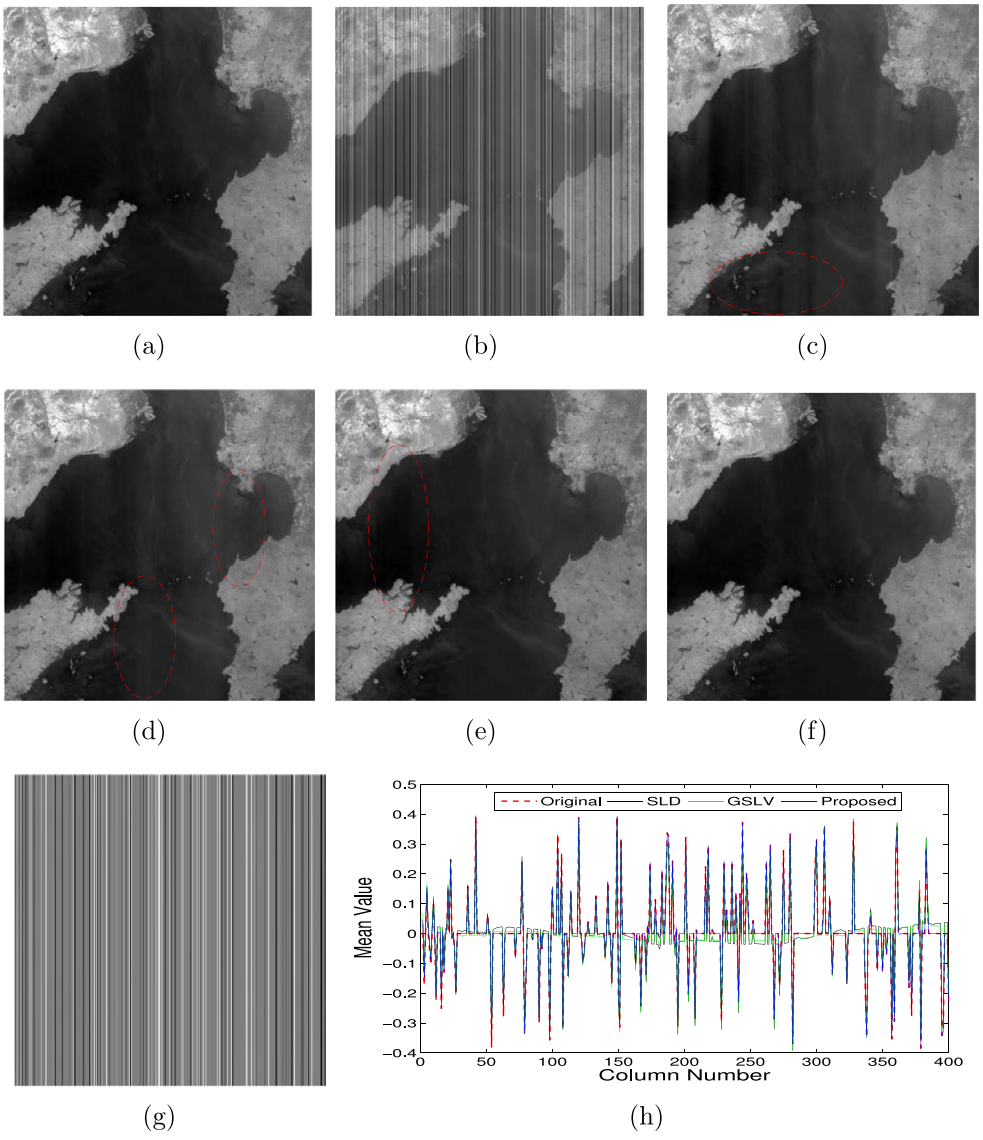

Fig. 3. Simulated destriping results for the nonperiodical stripes. (a) Original image; (b) stripe image; (c) WAFT; (d) SLD; (e) GSLV; (f) proposed method; (g) estimated stripe component by proposed method; (h) mean value comparison among the stripes estimated by proposed, SLD, GSLV, and the original one. Readers are recommended to zoom in all figures for better visibility.

thus

$$\mathbf{w}^{k+1} = \mathbf{shrink}\left(\nabla_x \mathbf{f} - \nabla_x \mathbf{s}^k + \frac{p_3^k}{\beta_3}, \frac{\lambda_2}{\beta_3}\right). \tag{15}$$

(3) Minimizing (10) with respect to $\mathbf{v}$ gives the following $\mathbf{v}$-subproblem

$$\mathbf{v} = \arg\min_{\mathbf{v}} \left\{ \lambda_1 \|\mathbf{v}\|_{2,1} + p_2^T(\mathbf{s}-\mathbf{v}) + \frac{\beta_2}{2}\|\mathbf{s}-\mathbf{v}\|_2^2 \right\}, \tag{16}$$

which has an approximated solution by the following soft-shrinkage formula [29]

$$\mathbf{v}_{g_i}^{k+1} = \max\left\{ \|r_i\|_2 - \frac{\lambda_1}{\beta_2}, 0 \right\} \frac{r_i}{\|r_i\|_2}, \quad r_i = \mathbf{s}_{g_i}^k + \frac{1}{\beta_2}\left(p_2^k\right)_{g_i}, \tag{17}$$

where g_i denotes each group of the image. Here, we regard each column of the image as a group.

(4) The $\mathbf{s}$ subproblem is described as follows

$$\mathbf{s} = \arg\min_{\mathbf{s}} \left\{ \frac{\beta_1}{2}\|\nabla_y \mathbf{s} - \mathbf{z} + \frac{p_1}{\beta_1}\|_2^2 + \frac{\beta_2}{2}\|\mathbf{s} - \mathbf{v} + \frac{p_2}{\beta_2}\|_2^2 + \frac{\beta_3}{2}\|\nabla_x \mathbf{f} - \nabla_x \mathbf{s} - \mathbf{w} + \frac{p_3}{\beta_3}\|_2^2 \right\}, \tag{18}$$

this is a quadratic optimization and differentiability. It is equivalent to solve the following linear system

$$\left(\beta_1 \nabla_y^T \nabla_y + \beta_2 + \beta_3 \nabla_x^T \nabla_x\right)\mathbf{s}^{k+1} = \beta_1 \nabla_y^T \left(\mathbf{z}^{k+1} - \frac{p_1^k}{\beta_1}\right) + \beta_2\left(\mathbf{v}^{k+1} - \frac{p_2^k}{\beta_2}\right) + \beta_3 \nabla_x^T\left(\nabla_x \mathbf{f} - \mathbf{w}^{k+1} + \frac{p_3^k}{\beta_3}\right). \tag{19}$$

In this work, we consider periodic boundary condition for $\mathbf{s}$, then $\nabla_y^T \nabla_y$ and $\nabla_x^T \nabla_x$ are block circulant matrices with circulant blocks. For the detailed discussion, we refer the reader to [39]. Therefor, the matrix on the left-hand side of (19) can be diagonalized by two-dimensional discrete Fourier transform $\mathcal{F}$. Using the convolution theorem of Fourier transforms, we can obtain the solution of $\mathbf{s}$ as follows

$$\mathbf{s}^{k+1} = \mathcal{F}^{-1}\left(\frac{\mathcal{A}}{\beta_1 \mathcal{F}(\nabla_y)^* \circ \mathcal{F}(\nabla_y) + \beta_2 + \beta_3 \mathcal{F}(\nabla_x)^* \circ \mathcal{F}(\nabla_x)}\right), \tag{20}$$

where $\mathcal{A} = \beta_1 \mathcal{F}(\nabla_y)^* \circ \mathcal{F}(\mathbf{z}^{k+1} - \frac{p_1^k}{\beta_1}) + \beta_2 \mathcal{F}(\mathbf{v}^{k+1} - \frac{p_2^k}{\beta_2}) + \beta_3 \mathcal{F}(\nabla_x)^* \circ \mathcal{F}(\nabla_x \mathbf{f} - \mathbf{w}^{k+1} + \frac{p_3^k}{\beta_3})$, "$*$" denotes complex conjugacy, "$\circ$" denotes component-wise multiplication, and the division is component-wise as well. $\mathcal{F}(\cdot)$ represents the fast Fourier transform and $\mathcal{F}^{-1}(\cdot)$ denotes its inverse transform.

Finally, the Lagrange multipliers p_1, p_2, and p_3 are updated in each iteration as follows

$$\begin{cases} p_1^{k+1} = p_1^k + \beta_1\left(\nabla_y \mathbf{s}^{k+1} - \mathbf{z}^{k+1}\right), \\ p_2^{k+1} = p_2^k + \beta_2\left(\mathbf{s}^{k+1} - \mathbf{v}^{k+1}\right), \\ p_3^{k+1} = p_3^k + \beta_3\left(\nabla_x \mathbf{f} - \nabla_x \mathbf{s}^{k+1} - \mathbf{w}^{k+1}\right). \end{cases} \tag{21}$$

From the above, we take advantage of the ADMM algorithm to separate the difficult optimization problem (7) into beforementioned four easy subproblems. The **z**, **v**, and **w** subproblems obtain approximate solutions by using the efficient soft-thresholding operator. Meanwhile, the **s** subproblem is a linear system, we can choose FFT to solve it efficiently. Moreover, the Lagrange multipliers p_1, p_2, and p_3 can be updated parallelly. The algorithm for solving our model (7) is summarized as Algorithm 1.

Algorithm 1 The proposed destriping algorithm.

1: **Input**: Stripe image **f**, parameters λ_1, λ_2, β_1, β_2, and β_3.
2: **Initialize**: Set $\mathbf{s}^0 = \mathbf{0}$, $\mathbf{z}^0 = \mathbf{v}^0 = \mathbf{0}$, $\mathbf{w}^0 = \nabla_y \mathbf{f}$, $p_1^0 = p_2^0 = p_3^0 = \mathbf{0}$, and $\varepsilon = 10^{-4}$.
3: **while** $\|(\mathbf{f} - \mathbf{s}^k) - (\mathbf{f} - \mathbf{s}^{k-1})\| / \|\mathbf{f} - \mathbf{s}^k\| > \varepsilon$ and $k < N_{\max}$ **do**
4: Solve $\mathbf{z}^{k+1}$, $\mathbf{v}^{k+1}$, $\mathbf{w}^{k+1}$ via (12), (17), and (15), respectively
5: Solve $\mathbf{s}^{k+1}$ by (20)
6: Update p_1^{k+1}, p_2^{k+1}, and p_3^{k+1} by (21).
7: **end while**
8: **Output**: $\mathbf{u}^{k+1} = \mathbf{f} - \mathbf{s}^{k+1}$.

3.3. Convergence analysis

In this subsection, we will illustrate the convergence of the proposed method. In fact, although there are four components in the constrained problem (9), they can be categorized as two parts. Actually, let

$$\mathbf{H} = \begin{pmatrix} \mathbf{z} \\ \mathbf{v} \\ \mathbf{w} \end{pmatrix}, \qquad \mathbf{G} = \mathbf{s}, \qquad g(\mathbf{H}) = \|\mathbf{z}\|_1 + \lambda_1 \|\mathbf{v}\|_{2,1} + \lambda_2 \|\mathbf{w}\|_1. \tag{22}$$

Then, (9) can be further expressed in a compact form

$$\arg\min_{\mathbf{H},\mathbf{G}} g(\mathbf{H}), \quad \text{subject to} \quad \mathbf{AH} + \mathbf{BG} = \mathbf{C}, \tag{23}$$

where **A**, **B**, and **C** are given by

$$\mathbf{A} = \begin{pmatrix} -\mathbf{I} & \mathbf{0} & \mathbf{0} \\ \mathbf{0} & -\mathbf{I} & \mathbf{0} \\ \mathbf{0} & \mathbf{0} & -\mathbf{I} \end{pmatrix}, \quad \mathbf{B} = \begin{pmatrix} \nabla_y \\ \mathbf{I} \\ -\nabla_x \end{pmatrix}, \quad \mathbf{C} = \begin{pmatrix} \mathbf{0} \\ \mathbf{0} \\ -\nabla_x \mathbf{f} \end{pmatrix}. \tag{24}$$

The problem (23) fits the framework of ADMM, and the resulting augmented Lagrangian function (10) can be rewritten as

$$\begin{aligned} &L(\mathbf{s}, \mathbf{z}, \mathbf{v}, \mathbf{w}) \\ &= \|\mathbf{z}\|_1 + \lambda_1 \|\mathbf{v}\|_{2,1} + \lambda_2 \|\mathbf{w}\|_1 \\ &\quad + \left\langle \begin{pmatrix} p_1 \\ p_2 \\ p_3 \end{pmatrix}, \begin{pmatrix} \nabla_y \\ \mathbf{I} \\ -\nabla_x \end{pmatrix} \mathbf{s} + \begin{pmatrix} -\mathbf{I} & \mathbf{0} & \mathbf{0} \\ \mathbf{0} & -\mathbf{I} & \mathbf{0} \\ \mathbf{0} & \mathbf{0} & -\mathbf{I} \end{pmatrix} \begin{pmatrix} \mathbf{z} \\ \mathbf{v} \\ \mathbf{w} \end{pmatrix} + \begin{pmatrix} \mathbf{0} \\ \mathbf{0} \\ \nabla_x \mathbf{f} \end{pmatrix} \right\rangle \\ &\quad + \frac{\beta}{2} \left\| \begin{pmatrix} \nabla_y \\ \mathbf{I} \\ -\nabla_x \end{pmatrix} \mathbf{s} + \begin{pmatrix} -\mathbf{I} & \mathbf{0} & \mathbf{0} \\ \mathbf{0} & -\mathbf{I} & \mathbf{0} \\ \mathbf{0} & \mathbf{0} & -\mathbf{I} \end{pmatrix} \begin{pmatrix} \mathbf{z} \\ \mathbf{v} \\ \mathbf{w} \end{pmatrix} + \begin{pmatrix} \mathbf{0} \\ \mathbf{0} \\ \nabla_x \mathbf{f} \end{pmatrix} \right\|_2^2, \end{aligned} \tag{25}$$

where p_1, p_2, and p_3 are the vectors corresponding to the Lagrange multipliers to the linear constraints, and β is the positive penalty parameter.

The optimization problem (25) is well structured since all the variable can be separated into two groups, **H** and **G**, and the variables **z**, **v**, and **w** are decoupled. Therefore, The convergence of the algorithm is theoretically guaranteed [32].

4. Experiment results

In the experiment, we employ two types of data, i.e., simulated data and real data, to compare the performance of our method with three state-of-the-art methods. The comparison methods include: filtering-based method [9] (WAFT), statistics-based method [16] (SLD) and optimization-based method [27] (GSLV). For the convenience of the parameter selection, the gray values of the stripe images are normalized to the domain [0, 1]. All experiments are run in MATLAB (R2014a) on a desktop of 8GB RAM, Inter (R) Core (TM) i5-4590 CPU, @3.30 GHz.

To give an overall evaluation, some qualitative and quantitative assessments are employed for comparison. For the experiments of simulated data, the qualitative indices include the visual performance and the mean cross-track profile. Moreover, we utilize two objective quantitative assessments, i.e., the peak signal-to-noise ratio (PSNR) and the structural similarity (SSIM) [40] http://www.ece.uwaterloo.ca/~z70wang/research/ssim/, which are full-reference evaluation indices. For the experiments of real data, since without ground-truth image as reference, we select the no-reference evaluation indices: noise reduction (NR) [17,18,25], mean relative deviation (MRD) [17,25,41], and image distortion (ID) [18,42]. NR is special for evaluating the global performance of destriping in the frequency domain. MRD is used to assess the performance of preserving the original healthy pixel in stripe-free regions, and ID is utilized to assess the distortion of destiping image. For the qualitative index, we choose power spectrum curve to show the destriping ability. Generally speaking, The large values of PSNR, SSIM, NR, and ID indices and lower MRD mean the better restored image.

Parameters selection: The proposed method involves two regularization parameters λ_1 and λ_2. To show the robustness of our model, we empirically fix the parameter $\lambda_1 = 0.001$ and the penalty parameters $\beta_1 = \beta_2 = \beta_3 = 0.1$. Since the dense levels of the stripe component is different, we empirically set $\lambda_2 \in [0.001, 0.1]$. For the compared methods, we have tried our best to tune their parameters according to the authors' suggestion in their papers to obtain the best results.

4.1. Simulated experiments

In our simulated experiments, we choose two kinds of stripe noise on two different ground truth images to confirm the effectiveness of the proposed method. Nonperiodical stripes in the MODIS image band 32 that is available from the website https://ladsweb.nascom.nasa.gov/, and periodical stripes in the IKONOS image which can be downloaded from on website https://openremotesensing.net/. Before simulated process, the clean images are coded to an 8-bit scale for showing convenience. Then the synthetic stripes with intensity [0, 255] are added into the clean image based on the degradation model (2). Finally, the simulated images are scaled into the interval [0, 1].

Nonperiodical stripes: Fig. 3(a) shows the original MODIS image band 32. To avoid the man-made influence, the location and the intensity value of each stripe line are randomly selected on the image, and Fig. 3(b) shows the results of stripe image. The destriping results of the four comparing methods are shown in Fig. 3. From Fig. 3(c), WAFT fails to remove the obvious stripes, since there are

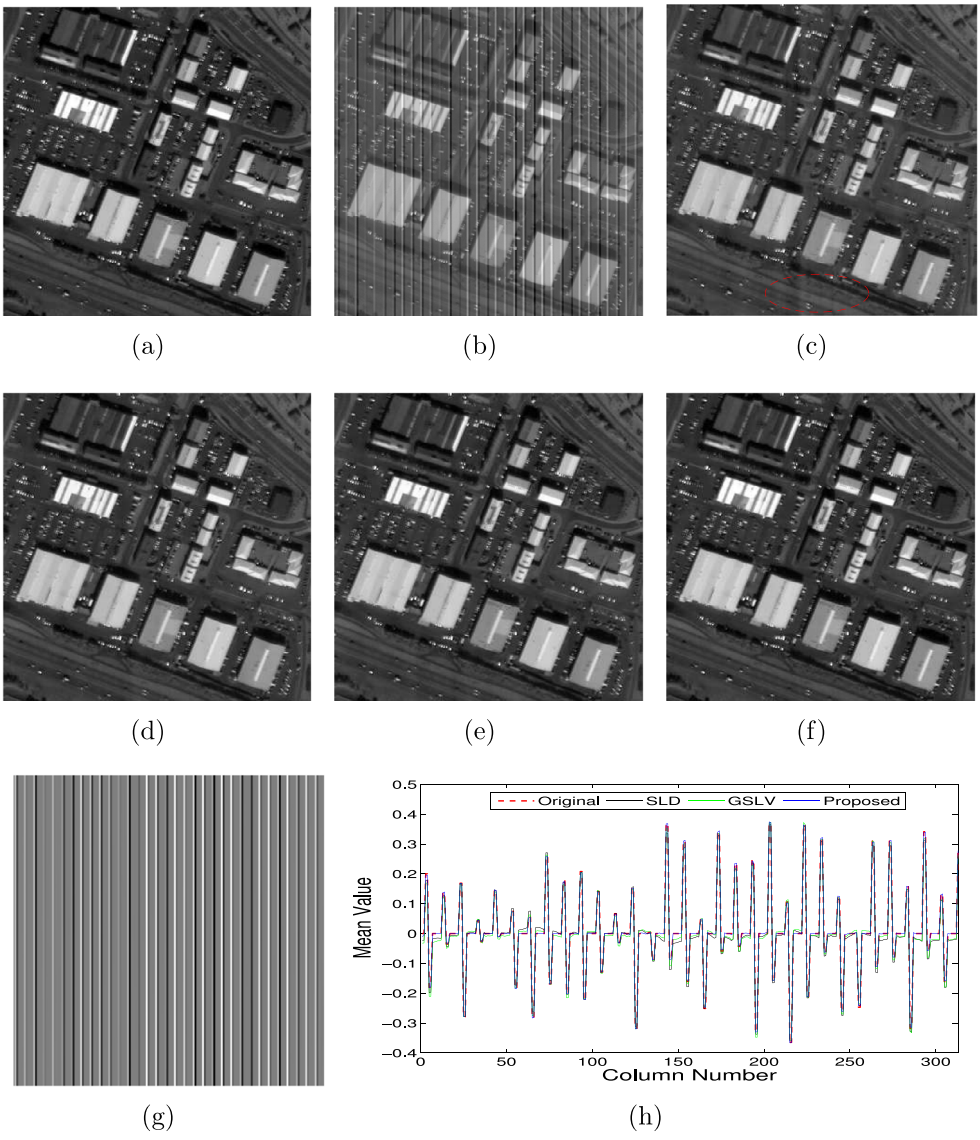

Fig. 4. Simulated destriping results for the periodical stripes. (a) Original image; (b) stripe image; (c) WAFT; (d) SLD; (e) GSLV; (f) proposed method; (g) estimated stripe component by proposed method; (h) mean value comparison among the stripes estimated by proposed, SLD, GSLV, and the original one. Readers are recommended to zoom in all figures for better visibility.(For interpretation of the references to color in this figure, the reader is referred to the web version of this article).

many residual stripes left, and it may result in blur effect in some regions. SLD method removes most evident stripes, but some artificial stripes are still existing as shown in Fig. 3(d). In Fig. 3(e), GSLV method can remove all stripes, but some pixel values of the stripe-free regions are destroyed. Comparing with the three methods, the proposed method obtains the best destriping results and shows the better visual performance in Fig. 3(f). Fig. 3(g) shows the stripe component which extracted by our method, it can be seen that the stripe-free areas information preserve well.

Since SLD, GSLV and the proposed method achieve destriping by estimating the stripe component, we compare the stripes estimated by the three methods with the real stripes. In Fig. 3(h), the horizontal axis denotes the column number, and the vertical axis stands for the mean value of stripe component. It is obvious that the two comparing methods lead to some minor errors at the stripe-free locations. In contrast, the stripe component estimated by our method is almost the same as the original stripes, it demonstrates that the proposed method has the ability of preserving stripe-free details in the remove stripes process.

Periodical stripes: To illustrate our method can be applied to various stripe noise, the periodical stripes are added to the ground-truth image. Fig. 4 shows the destriping results for the periodical stripes case. As displayed in Fig. 4(c), WAFT method fails to remove all stripes, with few stripes left in the image. SLD, GSLV, and the proposed method give the better visual results for destriping (see in Figs. 4(d)–(f)). However, in Fig. 4(h), we can find that SLD and GSLV methods fail to precisely estimate the stripe component, and they will result in blur effect and image details destroyed. The proposed method, in contrast, estimates the stripe component successfully, and also prevents extra background information loss.

Fig. 5 shows the mean cross-track profiles of the IKONOS image shown in Fig. 4 as an example. The horizontal axis represents the column number, and the vertical axis denotes the mean value of each image column. The red dotted line stands for the clean image, and the blue line is destriping results. Fig. 4 shows that the four comparing methods can almost completely remove stripe noise from the stripe image. However, in Fig. 5, it is clear to see

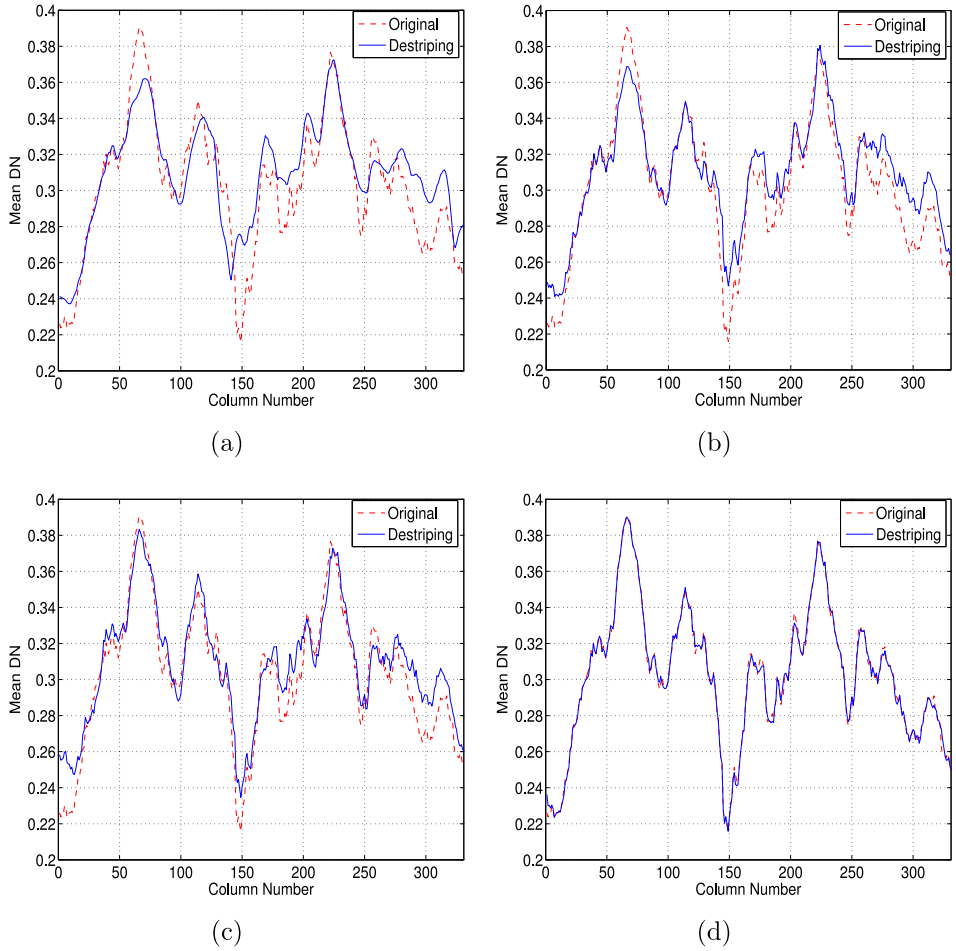

Fig. 5. Mean cross-track profiles of Fig. 4. (a) WAFT; (b) SLD; (c) GSLV; (d) proposed method.

Table 1
Quantitative results (PSNR (dB) and SSIM values) on simulated data.

Stripe noise	Case	Index	Degraded	WAFT	SLD	GSLV	Proposed
Nonperiodical	Case1	PSNR	23.05	35.45	36.77	38.12	**49.14**
		SSIM	0.656	0.985	0.994	0.996	**0.999**
	Case2	PSNR	18.27	32.94	33.05	34.47	**46.63**
		SSIM	0.310	0.982	0.994	0.996	**0.999**
Periodical	Case1	PSNR	20.68	37.18	38.47	38.09	**52.63**
		SSIM	0.588	0.989	0.993	0.994	**0.999**
	Case2	PSNR	17.67	35.02	37.43	38.04	**51.29**
		SSIM	0.458	0.987	0.995	0.994	**0.998**

that WAFT, SLD, and GSLV methods fail to precisely estimate the original image, which

indicates the destriping image distortion and blur problems. Unlike the three methods, the proposed method keeps a right curve tendency, and the column mean values of the destriping image are the same as the original image. It demonstrates that the proposed method can preserve stripe-free information and image details, as well as precisely estimate the stripe component. Table 1 shows the PSNR and SSIM values of simulated experiments, and the highest values are marked in bold. From the Table 1, it is clear that, in terms of the two indices, the proposed method obtains the best performance significantly.

4.2. Real experiments

In this subsection, we further test the real remote sensing stripe images to illustrate the efficiency of the proposed method. Two real stripe images with different stripe noise distributions downloaded from the website https://ladsweb.nascom.nasa.gov/ are selected to test. Fig. 6 shows the results of Terra MODIS image which is degraded by nonperiodical stripes. From Fig. 6(c), SLD method obtains a poor performance comparing with other methods, and many obvious stripes are still existing in the image. For WAFT and GSLV methods, the stripe noise is almost removed completely, but some residual stripes can be seen in the image. From Fig. 6(g), the proposed method successfully suppresses the stripe noise with fewer artifacts.

In addition, the results on Aqua MODIS image which is gravely degraded with periodical stripes are presented in Fig. 7. From Figs. 7(b)–(c), the destriping results obtained by WAFT and SLD show some residual stripes in the elliptical mark. As GSLV method, all stripes can be removed completely, but some regions are blurred in Fig. 7(d). Fig. 7(g) shows that the proposed method is better than the three comparing methods in term of removing stripes, preserving the stripe-free information and minimizing artifacts.

Fig. 8 shows the power spectrum of Aqua MODIS image shown in Fig. 7 as an example. The horizontal axis denotes the normalized frequency while the vertical axis represents the averaged power spectrum of all rows. Due to the influence of stripe noise, there are some impulses in the curve. After destriping, the impulses are greatly reduced. However, there still exist light burrs in the large impulses location in Fig. 8(a)–(c). It indicates that there are some residual stripes in WAFT, SLD and GSLV results, which is in accordance with Fig. 7(b)–(d). In Fig. 8(d), our method removes all the large impulses, meaning that all the stripes in the image are

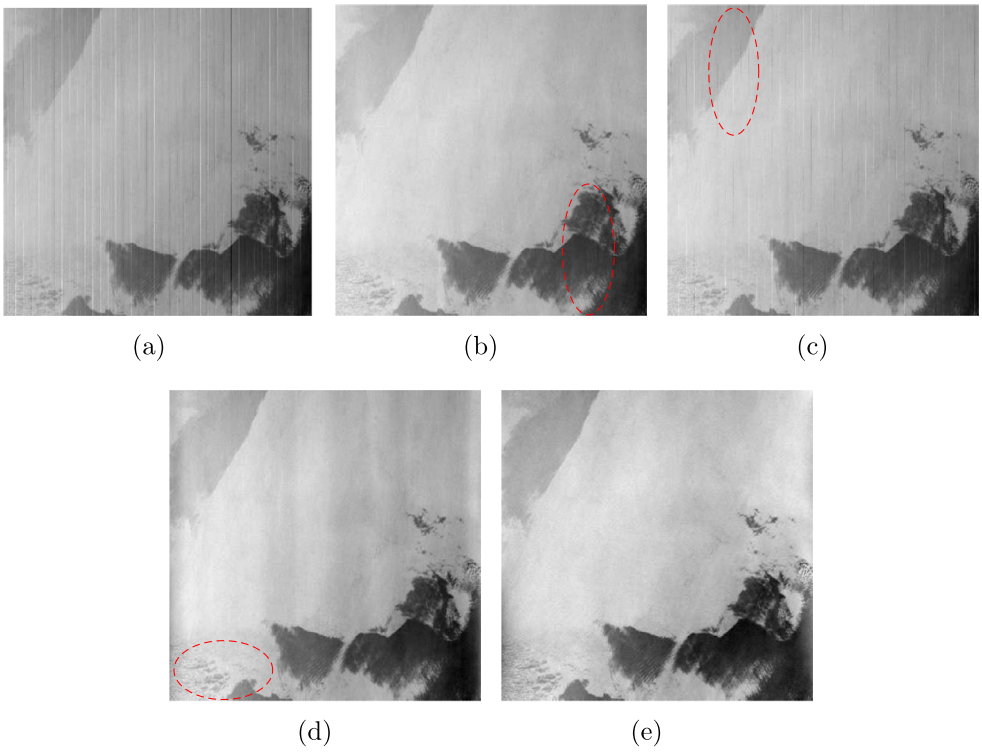

Fig. 6. Destriping results for the Terra MODIS image. (a) Original stripe image; (b) WAFT; (c) SLD; (d) GSLV; (e) proposed method.

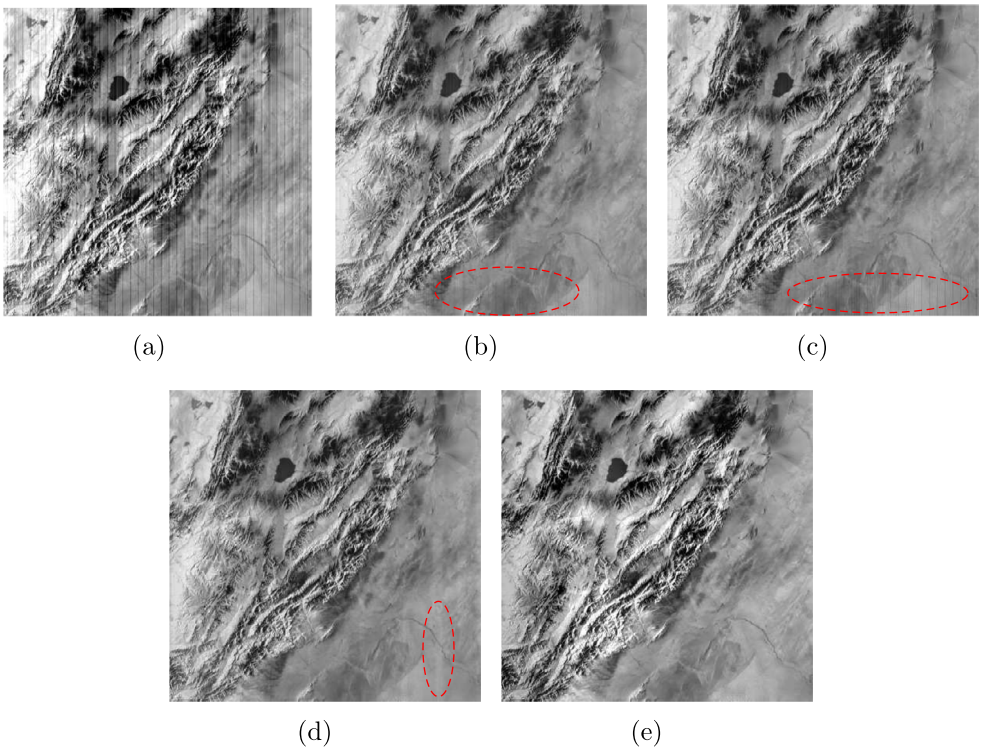

Fig. 7. Destriping results for the Aqua MODIS image. (a) Original stripe image; (b) WAFT; (c) SLD; (d) GSLV; (e) proposed method.

removed (see Fig. 7(e)). Furthermore, Table 2 lists the NR, MRD and ID values of real-data experiments. In particular, to avoid the influence of external factors, five 10×10 homogeneous regions are chosen to calculate MRD, then obtain the mean MRD. For NR and MRD indices, we can see that the proposed method achieves the better performances. As for ID index, the compared methods obtain the better results, the main reason is that these methods fail to remove stripes from original image so that retain original information. However, comparing with other methods, the proposed method can obtain better visual effect, and the ID index results are closer to one, which demonstrates that our method is an indeed competitive method.

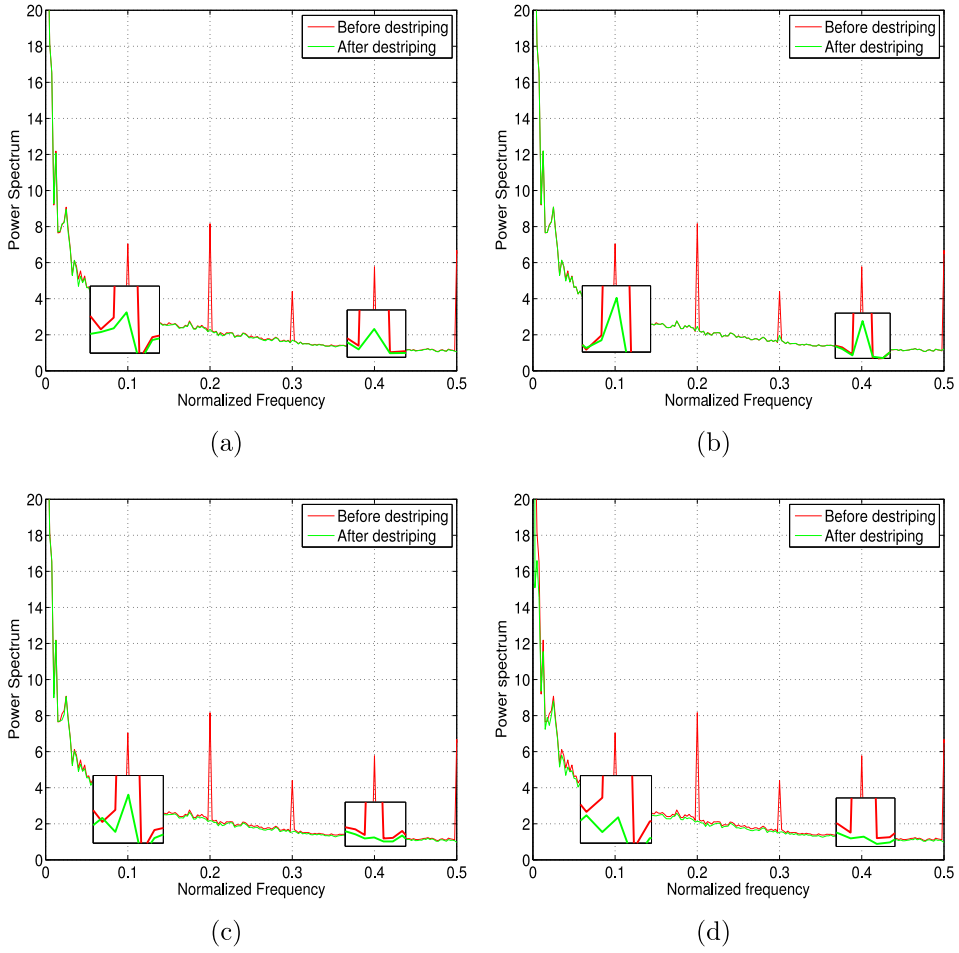

Fig. 8. Pow spectrum of Fig. 7. (a) WAFT; (b) SLD; (c) GSLV; (d) proposed method.

Table 2
Quantitative results on real data using NR, MRD, and ID.

Image	Index	WAFT	SLD	GSLV	Proposed
Terra MODIS image	NR	2.72	2.46	3.70	**3.94**
	MRD(%)	2.80	**1.47**	3.28	1.87
	ID	0.997	**0.999**	0.994	0.995
Aqua MODIS image	NR	3.31	2.99	3.47	**3.59**
	MRD(%)	4.88	3.66	5.25	**3.46**
	ID	0.998	**0.999**	0.996	0.991

4.3. Parameters analysis

To verify the robustness of key parameters to the performance of the proposed method, we give a sensitivity analysis for the two regularization parameters by using simulated experiment periodical stripes case 2 as an example. Fig. 9 plots the curves of the PSNR values as a function of the regularization parameters λ_1 and λ_2. From Fig. 9(a), we can see that the PSNR values of our method is robustness with the values of parameter λ_1 in the range of $0.5 \times 10^{-3} \sim 2.5 \times 10^{-3}$. In Fig. 9(b), the highest PSNR value is obtained with parameter λ_2 in the range of $0.3 \times 10^{-3} \sim 1 \times 10^{-3}$. Experimental results for other images show similar observations.

In our implementation, since all stripe component possess the column structure property, we empirically fix as $\lambda_1 = 0.001$. Due to the different dense levels of the stripe component in the test images, we empirically set the λ_2 with the range [0.001, 0.1]. For the positive penalty parameters, we empirically fix as $\beta_1 = \beta_2 = \beta_3 = 0.1$.

5. Conclusion

In this paper, we proposed a group sparsity based convex optimization model for remote sensing image destriping. Our model took full advantage of the directional and structural properties of stripe component, and utilized the group sparsity prior to well depict the structural property. The constraint of group sparsity term was more reasonable to separate and remove stripe noise, as well as preserved the background information of original images. After that, an efficient convex optimization solver, ADMM, was introduced to solve the proposed model. In particular, the algorithm convergence of the proposed convex model is guaranteed by the existing ADMM theory. Extensive experiments provided in this paper illustrated the state-of-the-art performance of the proposed method.

Nevertheless, there is still some space to improve the proposed method in the future. Our model can remove stripe for horizontal or vertical stripes efficiently, whereas for oblique stripes in georeferenced image, the property of column (or row) group sparsity does not exist. This is a shortcoming of our group sparsity model. In the future, we will focus on dividing groups for oblique stripes adaptively so that the improved method may overcome the mentioned shortcoming.

Acknowledgments

The authors would like to thank the anonymous reviewers and the Editor in Chief Prof. Steven Hoi for their constructive comments which helped to improve the quality of the paper. This

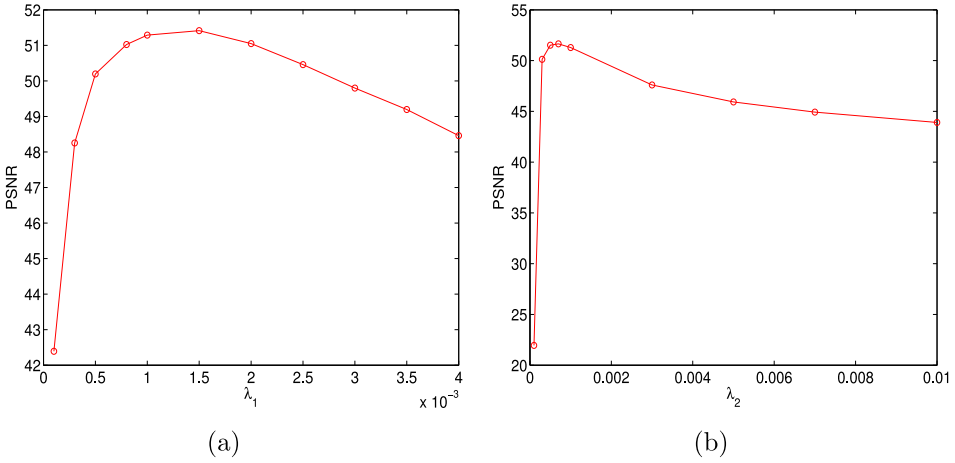

Fig. 9. (a) The PSNR curve as a function of parameter λ_1; (b) the PSNR curve as a function of parameter λ_2.

research is supported by 973 Program (2013CB329404), National Natural Science Foundation of China (NSFC) (61370147, 61402082), and the Fundamental Research Funds for the Central Universities (ZYGX2016J132).

References

[1] X.-L. Zhao, F. Wang, T.-Z. Huang, M.K. Ng, R.J. Plemmons, Deblurring and sparse unmixing for hyperspectral images, IEEE Trans. Geosci. Remote Sens. 51 (7) (2013) 4045–4058.
[2] H. Huang, Y. Huang, Improved discriminant sparsity neighborhood preserving embedding for hyperspectral image classification, Neurocomputing 136 (1) (2014) 224–234.
[3] B. Du, L. Zhang, D. Tao, D. Zhang, Unsupervised transfer learning for target detection from hyperspectral images, Neurocomputing 120 (10) (2013) 72–82.
[4] J. Chen, Y. Shao, H. Guo, W. Wang, B. Zhu, Destriping CMODIS data by power filtering, IEEE Trans. Geosci. Remote Sens. 41 (9) (2003) 2119–2124.
[5] J. Chen, C. Chang, Destriping of landsat MSS images by filtering techniques, Photogramm. Eng. Remote Sens. 58 (10) (1992) 1417–1423.
[6] J.J. Simpson, J.I. Gobat, R. Frouin, Improved destriping of GOES images using finite impulse response filters, Remote Sens. Environ. 52 (1) (1995) 15–35.
[7] J. Chen, H. Lin, Y. Shao, L. Yang, Oblique striping removal in remote sensing imagery based on wavelet transform, Int. J. Remote Sens. 27 (8) (2006) 1717–1723.
[8] J. Torres, S.O. Infante, Wavelet analysis for the elimination of striping noise in satellite images, Opt. Eng. 40 (7) (2001) 1309–1314.
[9] B. MŘnch, P. Trtik, F. Marone, M. Stampanoni, Stripe and ring artifact removal with combined wavelet!"fourier filtering, Opt. Express 17 (10) (2009) 8567–8591.
[10] R. Pande-Chhetri, A. Abd-Elrahman, De-striping hyperspectral imagery using wavelet transform and adaptive frequency domain filtering, ISPRS J. Photogramm. Remote Sens. 66 (5) (2011) 620–636.
[11] L. Sun, R. Neville, K. Staenz, H.P. White, Automatic destriping of hyperion imagery based on spectral moment matching, Can. J. Remote Sens. 34 (S1) (2008) S68–S81.
[12] M. Wegener, Destriping multiple sensor imagery by improved histogram matching, Int. J. Remote Sens. 11 (5) (1990) 859–875.
[13] P. Rakwatin, W. Takeuchi, Y. Yasuoka, Stripe noise reduction in MODIS data by combining histogram matching with facet filter, IEEE Trans. Geosci. Remote Sens. 45 (6) (2007) 1844–1856.
[14] F. Gadallah, F. Csillag, E. Smith, Destriping multisensor imagery with moment matching, Int. J. Remote Sens. 21 (12) (2000) 2505–2511.
[15] B.K. Horn, R.J. Woodham, Destriping landsat MSS images by histogram modification, Comput. Gr. Image Process 10 (1) (1979) 69–83.
[16] H. Carfantan, J. Idier, Statistical linear destriping of satellite-based pushbroom–type images, IEEE Trans. Geosci. Remote Sens. 48 (4) (2010) 1860–1871.
[17] H. Shen, L. Zhang, A MAP-based algorithm for destriping and inpainting of remotely sensed images, IEEE Trans. Geosci. Remote Sens. 47 (5) (2009) 1492–1502.
[18] M. Bouali, S. Ladjal, Toward optimal destriping of MODIS data using a unidirectional variational model, IEEE Trans. Geosci. Remote Sens. 49 (8) (2011) 2924–2935.
[19] Y. Chang, H. Fang, L. Yan, H. Liu, Robust destriping method with unidirectional total variation and framelet regularization, Opt. Express 21 (20) (2013) 23307–23323.
[20] Y. Zhang, G. Zhou, L. Yan, T. Zhang, A destriping algorithm based on TV-stokes and unidirectional total variation model, Optik 127 (1) (2016) 428–439.
[21] Y. Chang, L. Yan, H. Fang, C. Luo, Anisotropic spectral-spatial total variation model for multispectral remote sensing image destriping, IEEE Trans. Image Process 24 (6) (2015) 1852–1866.
[22] M. Wang, X. Zheng, J. Pan, B. Wang, Unidirectional total variation destriping using difference curvature in MODIS emissive bands, Infrared Phys. Technol. 75 (2016) 1–11.
[23] G. Zhou, H. Fang, C. Lu, S. Wang, Z. Zuo, J. Hu, Robust destriping of MODIS and hyperspectral data using a hybrid unidirectional total variation model, Optik 126 (7) (2015) 838–845.
[24] W. He, H. Zhang, L. Zhang, H. Shen, Total-variation-regularized low-rank matrix factorization for hyperspectral image restoration, IEEE Trans. Geosci. Remote Sens. 54 (1) (2016) 178–188.
[25] X. Lu, Y. Wang, Y. Yuan, Graph-regularized low-rank representation for destriping of hyperspectral images, IEEE Trans. Geosci. Remote Sens. 51 (7) (2013) 4009–4018.
[26] H. Zhang, W. He, L. Zhang, H. Shen, Q. Yuan, Hyperspectral image restoration using low-rank matrix recovery, IEEE Trans. Geosci. Remote Sens. 52 (8) (2014) 4729–4743.
[27] X. Liu, X. Lu, H. Shen, Q. Yuan, Y. Jiao, L. Zhang, Stripe noise separation and removal in remote sensing images by consideration of the global sparsity and local variational properties, IEEE Trans. Geosci. Remote Sens. 54 (5) (2016) 3049–3060.
[28] W. Zuo, D. Meng, L. Zhang, X. Feng, D. Zhang, A generalized iterated shrinkage algorithm for non-convex sparse coding, in: Proceedings of the ICCV, 2013, pp. 217–224.
[29] W. Deng, W. Yin, Y. Zhang, Group sparse optimization by alternating direction method, in: Proceedings of the SPIE Optical Engineering+ Applications, 2013 88580R-88580R-15.
[30] J. Eckstein, D.P. Bertsekas, On the Douglas-Rachford splitting method and the proximal point algorithm for maximal monotone operators, Math. Program. 55 (1) (1992) 293–318.
[31] R. Glowinski, Lectures on Numerical Methods for Non-Linear Variational Problems, Springer Science & Business Media, 2008.
[32] S. Boyd, N. Parikh, E. Chu, B. Peleato, J. Eckstein, Distributed optimization and statistical learning via the alternating direction method of multipliers, Found. Trends® in Mach. Learn. 3 (1) (2011) 1–122.
[33] L.-J. Deng, W. Guo, T.-Z. Huang, Single image super-resolution by approximated heaviside functions, Inf. Sci. 348 (2016) 107–123.
[34] X.-L. Zhao, W. Wang, T.-Y. Zeng, T.-Z. Huang, M.K. Ng, Total variation structured total least squares method for image restoration, SIAM J. Sci. Comput. 35 (6) (2013) B1304–B1320.
[35] J. Liu, T.-Z. Huang, I.W. Selesnick, X.-G. Lv, P.-Y. Chen, Image restoration using total variation with overlapping group sparsity, Inf. Sci. 295 (2015) 232–246.
[36] G. Liu, T.-Z. Huang, J. Liu, High-order TVL1-based images restoration and spatially adapted regularization parameter selection, Comput. Math. Appl. 67 (2014) 2015–2026.
[37] X.L. Zhao, F. Wang, M.K. Ng, A new convex optimization model for multiplicative noise and blur removal, SIAM J. Imaging Sci. 7 (7) (2014) 456–475.
[38] D.L. Donoho, De-noising by soft-thresholding, IEEE Trans. Inf. Theory 41 (3) (1995) 613–627.
[39] M.K. Ng, R.H. Chan, W.C. Tang, A fast algorithm for deblurring models with Neumann boundary conditions, SIAM J. Sci. Comput. 21 (3) (1999) 851–866.
[40] Z. Wang, A.C. Bovik, H.R. Sheikh, E.P. Simoncelli, Image quality assessment: from error visibility to structural similarity, IEEE Trans. Image Process. 13 (4) (2004) 600–612.
[41] N. Acito, M. Diani, G. Corsini, Subspace-based striping noise reduction in hyperspectral images, IEEE Trans. Geosci. Remote Sens. 49 (4) (2011) 1325–1342.
[42] M. Bouali, S. Ladjal, A variational approach for the destriping of MODIS data, IGARSS (2010) 2194–2197.

Yong Chen received the B.S. degree from the East China University of Technology, Nanchang, China, in 2015. He is currently working toward the M.S. degree with the School of Mathematical Sciences, University of Electronic Science and Technology of China (UESTC), Chengdu, China. His research interests include remote sensing image processing and sparse optimization.

Ting-Zhu Huang received the B. S., M. S., and Ph. D. degrees in Computational Mathematics from the Department of Mathematics, Xi'an Jiaotong University, Xi'an, China. He is currently a professor in the School of Mathematical Sciences, UESTC. He is currently an editor of The Scientific World Journal, Advances in Numerical Analysis, J. Appl. Math., J. Pure and Appl. Math.: Adv. and Appl., J. Electronic Sci. and Tech. of China, etc. His current research interests include scientific computation and applications, numerical algorithms for image processing, numerical linear algebra, preconditioning technologies, and matrix analysis with applications, etc.

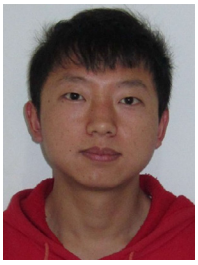

Liang-Jian Deng received B.S. and Ph.D. degrees from the School of Mathematical Sciences, University of Electronic Science and Technology of China (UESTC), in 2010 and 2016, respectively. From Sept. 2013 to Sept. 2014, he followed Prof. Weihong Guo at Case Western Reserve University (CWRU), Cleveland, USA, as a Joint-Training Ph.D. student. He is currently a lecturer of the School of Mathematical Sciences in UESTC. His research interest is now image processing, including natural image processing and remote sensing image processing, e.g., super-resolution, fusion, destriping, unmixing, inpainting, etc.

Xi-Le Zhao received the M.S. and Ph.D. degrees from the University of Electronic Science and Technology of China (UESTC), Chengdu, China, in 2009 and 2012. Currently, he is an associate professor with the School of Mathematical Sciences, UESTC. His main research interests are focused on image processing and sparse optimization.

Min Wang received B.S. degree from the School of Mathematical Sciences, University of Electronic Science and Technology of China (UESTC), Chengdu, China, in 2012. He is currently pursuing the Ph.D. degree with School of Mathematical Sciences of UESTC. His current research interest is image processing, data integration.